Journal of Sound and Vibration xxx (xxxx) xxx

Contents lists available at ScienceDirect

Journal of Sound and Vibration

journal homepage: www.elsevier.com/locate/jsv

Generalized dispersive mode decomposition: Algorithm and applications

Shiqian Chen[a,*], Kaiyun Wang[a], Zhike Peng[b], Chao Chang[a], Wanming Zhai[a]

[a] State Key Laboratory of Traction Power, Southwest Jiaotong University, Chengdu 610031, China
[b] State Key Laboratory of Mechanical System and Vibration, Shanghai Jiao Tong University, Shanghai 200240, China

ARTICLE INFO

Article history:
Received 26 June 2020
Revised 27 September 2020
Accepted 17 October 2020

Keywords:
Group delay
Dispersion curve
Fault diagnosis
Lamb wave
Time-frequency (TF)

ABSTRACT

Dispersive signals known for frequency-dependent characteristics have been frequently encountered in various fields like nondestructive testing, underwater acoustics, etc. Such signals often exhibit frequency-varying group delays (GDs) and consist of multiple modes overlapped in the time-frequency (TF) domain, which brings challenges to existing signal processing methods. In this paper, a generalized dispersive mode decomposition (GDMD) method is proposed to accurately estimate GDs and fully separate overlapped modes of dispersive signals. Specifically, a generalized dispersive signal model is defined in the frequency domain at first. Then, based on the defined model, the mode decomposition issue is formulated as an optimal dispersion compensation problem where the method simultaneously searches for the optimal modes and their GDs, with which the dispersion effects of all the modes can be fully eliminated. In addition, according to the output results of the GDMD, a high-quality TF distribution can be constructed to clearly reveal the TF pattern of a multimodal dispersive signal. Simulated examples and real-life applications to railway wheel fault diagnosis and Lamb wave analysis are carried out to show the effectiveness of the GDMD.

1. Introduction

Dispersive signals have been widely investigated in various fields, such as structure health monitoring [1,2] nondestructive testing [3–5], underwater acoustics [6,7] and biomedical applications [8,9]. Dispersive signals exhibit frequency-dependent characteristics, among which the group delay (GD), defined as the derivative of the phase function with respect to the frequency, is the most important one [10,11]. GD contains valuable information about the source and system and thus can be utilized for source localization and system identification. However, when a broadband signal passes through a nonlinear system, different time delays will be generated at each frequency, resulting in a frequency-varying GD. In addition, practical dispersive signals like guided waves [12] often contain multiple signal modes with crossed GD curves (also known as dispersion curves), which makes it difficult for signal analysis. Therefore, accurately separating these crossed dispersive modes and extracting their GD curves are crucial for practical applications.

Dispersive signal is a kind of typical non-stationary signal with time-varying or frequency-varying signal features. Time-frequency analysis (TFA) is one of the most effective methods for non-stationary signal processing since it can characterize signal features in both time and frequency domains simultaneously. Conventional TFA methods like short-time Fourier

* Corresponding author.
E-mail address: chenshiqian@swjtu.edu.cn (S. Chen).

https://doi.org/10.1016/j.jsv.2020.115800

transform (STFT) and continuous wavelet transform have been widely used in various fields, however, the time-frequency distributions (TFDs) obtained by these methods are usually subjected to poor energy concentration. Quadratic TFA methods like Wigner-Ville distribution are known for fine concentration but they often suffer from cross-terms for nonlinear and multimodal signals. To improve the readability and concentration of a TFD, researchers proposed a post-processing technique called time-frequency (TF) reassignment [13] which moves the TF coefficients from their original locations to the local energy centroids so as to sharpen the TFD. As a special case of the TF reassignment, synchrosqueezing transform (SST) [14] has attracted considerable attention since it can not only enhance the TFD but also inherit the invertibility for signal reconstruction. However, SST may still generate blurry TFDs for fast-varying signals as it essentially performs zero-order approximation for signals. To address this issue, demodulation techniques [15–17] or higher-order approximation operators [18,19] have been employed to improve the fast-signal-characterizing ability of SST. On the other hand, SST only reassigns the TF coefficients along frequency axis and thus is less capable of analyzing impulsive-like signals or dispersive signals with transient behaviors. To reduce the energy diffusion along time axis for transient signals, some researchers further developed time-reassigned SST [20,21] and horizontal SST [22]. One major limitation of the current SST-based methods is that they cannot resolve close or crossed signal modes since the TF coefficients of these modes are almost overlapped and thus cannot be properly reassigned. In addition, noise interference may change the local TF energy centroids, which will directly affect the SST results.

Parameterized TFA methods are another type of popular TF methods which are known for the signal-dependent resolution. Such methods assume that the signal can be characterized by a parameterized model and then formulate the TFA issue as a parameter estimation problem. When the defined model well matches with the signal, the best TF resolution can be achieved by the TF methods. Yang et al. [23] proposed a general parameterized TF transform (GPTFT) which employs different models like polynomial, spline and Fourier series to characterize the instantaneous frequency (IF) of the signal. Moreover, to estimate the GD of a dispersive signal, the frequency-domain GPTFT as a dual version of the original method was also developed [10]. However, a set of parameters can only match with a certain signal mode when each mode exhibits different TF patterns. Therefore, GPTFT cannot completely characterize a multimodal signal in one execution. One possible solution is to employ image filtering techniques to assemble TFDs generated by multiple executions of the GPTFT (with respect to different modes) to form a multimodal TFD [11]. Analogously, in some specific applications of dispersion analysis, researchers employ particular dispersion models to construct effective parameterized TF methods like dispersion-based STFT [24] and dispersive Radon transform [25]. Clearly, one shortcoming of the parameterized methods is that they cannot be applied in more general cases where the predefined model mismatches with the considered signal.

The methods mentioned above mainly focus on the TF representation of the signal. Of particular interest to us are the signal-decomposition-based TFA methods which can extract inherent modes underlying a signal and thus clearly reveal the TF patterns of the signal. In the past decades, researchers have developed many famous signal decomposition methods like empirical mode decomposition, empirical wavelet transform, variational mode decomposition, etc., most of which are subjected to narrowband conditions [26,27]. These methods often suffer from over-decomposition issues (i.e., the same signal mode is split into different parts) when dealing with wideband signals (e.g., FM signals). Recently, Chen et al. proposed several chirp-model-based signal decomposition methods like variational nonlinear chirp mode decomposition (VNCMD) [28] and adaptive chirp mode decomposition (ACMD) [29,30] to analyze multimodal wideband chirp signals. One promising advantage of such methods is that they can accurately estimate IFs and instantaneous amplitudes of close or even crossed signal modes, and therefore a quality TFD of the signal can be constructed [31]. Nevertheless, these methods are not applicable for dispersive signal analysis since the chirp model is not able to characterize the dispersion effect. For dispersive signal decomposition, the dispersion compensation method (DCM) [32,33] has aroused much interest. With the DCM, a dispersive signal with a frequency-varying GD can be transformed into a transient impulse (with a constant GD) which can thus be separated by a short-time rectangular window. It deserves to be mentioned that the SST-based method has also been reported for dispersive signal separation [34]. However, neither the DCM nor the SST-based methods can separate dispersive modes overlapped in the TF domain.

In summary, there is still a lack of a generalized signal decomposition method which can deal with crossed or overlapped dispersive modes. Motivated by the ACMD with the advantage in separating wideband chirp modes, a generalized dispersive mode decomposition (GDMD) method is developed. This work mainly includes two contributions: 1) considering the frequency-dependent dispersive characteristics, a generalized (non-parametric) dispersive signal model defined in the frequency domain is introduced; 2) based on the defined model, a joint-estimation algorithm is presented to accurately estimate GDs of crossed dispersive modes and then achieve the mode separation. In fact, the proposed GDMD can be regarded as an optimal DCM where the optimal GDs are estimated such that the dispersion effects of all the modes can be fully eliminated with the estimation results. In addition, different from the conventional DCM, thanks to the joint-estimation algorithm, the energies of the crossed modes near the intersections can be well balanced, leading to accurate mode reconstruction results.

The rest of the paper is organized as follows. After a brief description of the chirp signal model, the ACMD is introduced in Section 2. The proposed GDMD method is detailed in Section 3. Numerical examples are presented in Section 4 and then real-life applications of the GDMD are carried out in Section 5. Section 6 concludes the paper.

2. Theoretical background

2.1. Chirp signal model

A general chirp signal often has a time-varying amplitude and frequency, and therefore the AM-FM signal model can be employed to represent such signal as [29]:

$$s(t) = a(t)\cos\left[2\pi\int_0^t f(\lambda)\mathrm{d}\lambda + \phi\right] \tag{1}$$

where $a(t)$, $f(t)$and ϕstand for the instantaneous amplitude, IF, and initial phase of the chirp signal, respectively. By introducing a demodulation frequency $\bar{f}(t)$, Eq. (1)can be rewritten as:

$$s(t) = c(t)\cos\left[2\pi\int_0^t \bar{f}(\lambda)\mathrm{d}\lambda\right] + d(t)\sin\left[2\pi\int_0^t \bar{f}(\lambda)\mathrm{d}\lambda\right] \tag{2}$$

with

$$\begin{cases} c(t) = a(t)\cos\left\{2\pi\int_0^t\left[f(\lambda) - \bar{f}(\lambda)\right]\mathrm{d}\tau + \phi\right\} \\ d(t) = -a(t)\sin\left\{2\pi\int_0^t\left[f(\lambda) - \bar{f}(\lambda)\right]\mathrm{d}\tau + \phi\right\} \end{cases} \tag{3}$$

where $c(t)$and $d(t)$are referred to as demodulated signals. Clearly, if let $\bar{f}(t) = f(t)$, the demodulated signals will be transformed into slowly-varying baseband signals.

2.2. Adaptive chirp mode decomposition

As defined in Eq. (1), the chirp signal is usually a wideband signal due to the FM effect (i.e., the IF $f(t)$may vary in a wide range). Conventional signal decomposition methods like EMD and VMD are developed based on narrowband signal conditions, and thus may not properly analyze chirp signals. To deal with this challenging issue, the ACMD method was developed in [29]. More concretely, as shown in Eq. (3), if a proper demodulation frequency $\bar{f}(t)$is specified, the FM effect and the bandwidth of the demodulated signals will be effectively reduced. Therefore, the idea of the ACMD is to find the optimal demodulation frequency (i.e., the IF $f(t)$) by minimizing the bandwidth of the demodulated signals.

Assuming that the collected signal $s(t)$is composed of multiple signal modes, the ACMD extracts the i th mode $s_i(t)$and estimates its IF $f_i(t)$by solving the optimization problem as:

$$\begin{aligned} &\min_{c_i(t), d_i(t), \bar{f}_i(t)} \left\{\left\|c_i''(t)\right\|_2^2 + \left\|d_i''(t)\right\|_2^2 + \alpha\left\|s(t) - s_i(t)\right\|_2^2\right\} \\ &\text{with } s_i(t) = c_i(t)\cos\left[2\pi\int_0^t \bar{f}_i(\lambda)\mathrm{d}\lambda\right] + d_i(t)\sin\left[2\pi\int_0^t \bar{f}_i(\lambda)\mathrm{d}\lambda\right] \end{aligned} \tag{4}$$

where the square of the $l_2$norm of the second derivative (i.e., $\|c_i''(t)\|_2^2$and $\|d_i''(t)\|_2^2$) is calculated to measure the signal smoothness which can also reflect the signal bandwidth [35]; $\alpha > 0$ is a weighting factor. Essentially, formula (4) is indicative of a greedy algorithm like the matching pursuit [36] which searches for the optimal mode by minimizing the residual energy (i.e., $\|s(t) - s_i(t)\|_2^2$). After extracting the ith mode $s_i(t)$by solving Eq. (4), one can remove the obtained mode from the original signal, i.e., $s(t) = s(t) - s_i(t)$, and then repeat the algorithm (to the residual signal) to extract other modes. Note that the ACMD is designed to analyze time-varying characteristics like IF for the chirp signal and thus cannot properly deal with frequency-varying characteristics like GD for the dispersive signal.

3. Generalized dispersive mode decomposition

3.1. Dispersive signal model

The decomposition issue of a multimodal dispersive signal is considered in this study. For the proposed GDMD method, the base function is the so-called generalized dispersive mode (GDM) which can effectively characterize the dispersion properties of a dispersive signal. Considering the frequency-dependent characteristics, the GDM is defined in the frequency domain as:

Definition 1. A function $s(t)(\mathbb{R} \to \mathbb{R})$ is referred to as the GDM if its Fourier transform $S(f) = \int_{-\infty}^{\infty} s(t)\exp(-\mathrm{j}2\pi ft)\mathrm{d}t$can be expressed as:

$$S(f) = A(f)\exp\left\{-\mathrm{j}\left[2\pi\int_0^f \tau(\lambda)\mathrm{d}\lambda + \varphi\right]\right\} \tag{5}$$

with $A(f)$and $\tau(f)$satisfying the following conditions:

$A \in C^1(\mathbb{R}) \cap L^\infty(\mathbb{R}),\ \tau \in C^1(\mathbb{R})$

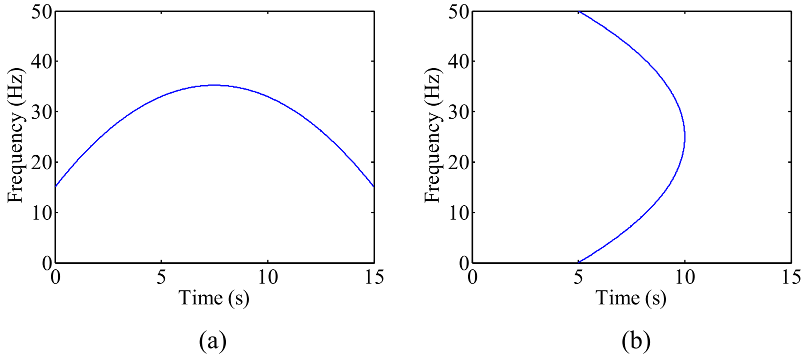

Fig. 1. Illustration of (a) IF and (b) GD.

$$\inf_{f\in\mathbb{R}} A(f) > 0,\ \inf_{f\in\mathbb{R}} \tau(f) > 0$$

$$\sup_{f\in\mathbb{R}} \tau(f) < \infty,\ \sup_{f\in\mathbb{R}} \left|\tau'(f)\right| < \infty$$

$$\left|A'(f)\right|, \left|\tau'(f)\right| \le \varepsilon,\ \forall f \in \mathbb{R}$$

where $\mathrm{j} = \sqrt{-1}$, $f$stands for the frequency variable; $A(f)$, $\tau(f)$, and φdenote the amplitude, the so-called GD, and the initial phase of the frequency-domain signal $S(f)$, respectively; $\varepsilon > 0$ controls the change rates of $A(f)$and $\tau(f)$. Note that a minus sign is added in front of the phase function of Eq. (5)to reflect the time-delay property. Eq. (5) indicates that the GDM can effectively characterize the frequency-varying amplitude and GD.

Practical dispersive signals often contain multiple modes and contaminated by environmental noise, and thus can be represented as:

$$\begin{aligned} S(f) &= \sum_{i=1}^{M} S_i(f) + \eta(f) \\ &= \sum_{i=1}^{M} A_i(f) \exp\left\{-\mathrm{j}\left[2\pi \int_0^f \tau_i(\lambda)\mathrm{d}\lambda + \varphi_i\right]\right\} + \eta(f) \end{aligned} \tag{6}$$

where M is the number of the dispersive modes, $S_i(f)$denotes the i th mode defined in Eq. (5), $\eta(f)$is the noise. By introducing auxiliary time delays $\bar{\tau}_i(f)$for $i = 1, \cdots, M$, Eq. (6)can be rewritten as:

$$S(f) = \sum_{i=1}^{M} G_i(f) \exp\left[-\mathrm{j}2\pi \int_0^f \bar{\tau}_i(\lambda)\mathrm{d}\lambda\right] + \eta(f) \tag{7}$$

with

$$G_i(f) = A_i(f) \exp\left\{-\mathrm{j}\left\{2\pi \int_0^f [\tau_i(\lambda) - \bar{\tau}_i(\lambda)]\mathrm{d}\lambda + \varphi_i\right\}\right\} \tag{8}$$

Note that, similar to the frequency demodulation in Eq. (3), Eq. (8) indicates the dispersion compensation [32] and $\bar{\tau}_i(f)$is the compensation amount. Ideally, when $\bar{\tau}_i(f) = \tau_i(f)$, the dispersion effect of $G_i(f)$will be fully eliminated, resulting in a transient impulse (with a very short duration) located at $\tau = 0$.

***Remark*:** There exists a clear dual relation between the chirp signal model (in Eq. (1)) and the proposed GDM (in Eq. (5)). The former is for the time-varying signal feature (like IF) modeling while the latter is for the frequency-varying dispersion feature (like GD) modeling. Both of them have a wide range of applications. Fig. 1 illustrates a typical IF and GD. As mentioned above, the GDM can not only model broadband dispersive signals like guided waves but also transient impulse signals (i.e., the GD is nearly constant and the TF pattern is a line nearly parallel to the frequency axis) which have been extensively studied in machine fault diagnosis [37–39]. In addition, different from most existing methods like SST [14] which impose separation conditions on the signal modes, we consider a general case that the dispersive modes in Eq. (6) may overlap in the TF domain.

3.2. Formulation and algorithm

As discussed above, the DCM can be used to reduce the dispersion effect and thus reduce the effective time duration of a dispersive signal. Therefore, the proposed GDMD is formulated as an optimal DCM where the optimal GD is estimated

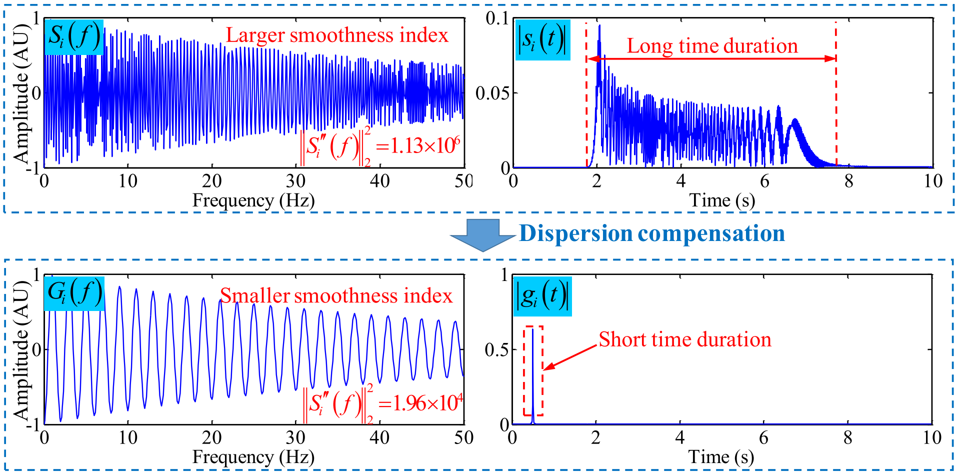

Fig. 2. Illustration of the dispersion compensation principle of the GDMD (top figures show the frequency and time domain waveforms of a dispersive signal; bottom figures show the waveforms after dispersion compensation; herein the real parts of the frequency-domain waveforms are given).

such that the signal (i.e., $G_i(f)$in Eq. (8)) has the shortest time duration (i.e., becomes a purely transient impulse) after dispersion compensation. Moreover, to deal with overlapped modes, a high-resolution joint-estimation scheme is adopted to estimate all the signal modes simultaneously. This scheme can accurately distribute energies of the overlapped modes at the intersections. Specifically, the GDMD is formulated as:

$$\min_{\{G_i(f)\},\{\bar{\tau}_i(f)\}}\left\{\sum_{i=1}^{M}\left\|G_i''(f)\right\|_2^2+\alpha\left\|S(f)-\sum_{i=1}^{M}S_i(f)\right\|_2^2\right\}$$
$$\text{with } S_i(f)=G_i(f)\exp\left[-\mathrm{j}2\pi\int_0^f\bar{\tau}_i(\lambda)\mathrm{d}\lambda\right] \tag{9}$$

Inspired by the ACMD defined in Eq. (4), the GDMD also uses the squared $l_2$norm of the second derivative to measure the smoothness of the frequency-domain signals and also evaluate their durations in the time domain. Fig. 2 illustrates the dispersion compensation principle of the GDMD.

For the algorithm implementation, it is assumed that the frequency-domain signal is sampled at $f=f_0,\cdots f_{N-1}$where N is the number of the frequency bins, and then formula (9) can be written in the matrix form as:

$$\min_{\boldsymbol{g},\boldsymbol{K}}\left[\mathcal{J}_\alpha(\boldsymbol{g},\boldsymbol{K})\right]=\min_{\boldsymbol{g},\boldsymbol{K}}\left\{\|\boldsymbol{\Psi}\boldsymbol{g}\|_2^2+\alpha\|\boldsymbol{s}-\boldsymbol{K}\boldsymbol{g}\|_2^2\right\} \tag{10}$$

where $\boldsymbol{s}=[S(f_0),\cdots,S(f_{N-1})]^T$, $\boldsymbol{g}=[(\boldsymbol{g}_1)^T,\cdots,(\boldsymbol{g}_M)^T]^T$, $\boldsymbol{g}_i=[G_i(f_0),\cdots,G_i(f_{N-1})]^T$, for$i=1,\cdots,M$, superscript Tstands for the transposition, the kernel matrix $\boldsymbol{K}$is given as:

$$\boldsymbol{K}=[\boldsymbol{K}_1,\cdots,\boldsymbol{K}_M] \tag{11}$$

where $\boldsymbol{K}_i$for $i=1,\cdots,M$are diagonal matrixes represented as:

$$\boldsymbol{K}_i=\mathrm{diag}[\exp[-\mathrm{j}\theta_i(f_0)],\cdots,\exp[-\mathrm{j}\theta_i(f_{N-1})]] \tag{12}$$

where $\theta_i(f)=2\pi\int_0^f\bar{\tau}_i(\lambda)\mathrm{d}\lambda$. The matrix $\boldsymbol{\Psi}$in Eq. (10) conducts the second-order difference operations for the M dispersive modes as:

$$\boldsymbol{\Psi}=\mathrm{diag}\underbrace{[\boldsymbol{\Lambda},\cdots,\boldsymbol{\Lambda}]}_{M\text{matrixes}} \tag{13}$$

where $\boldsymbol{\Lambda}$is a second-order difference matrix.

An iterative algorithm is introduced to solve the optimization problem in Eq. (10). In the n-th iteration, by setting the gradient of Eq. (10) to zero, the vector $\boldsymbol{g}$can be updated as:

$$\boldsymbol{g}^{(n+1)}=\begin{bmatrix}\boldsymbol{g}_1^{(n+1)}\\ \vdots\\ \boldsymbol{g}_M^{(n+1)}\end{bmatrix}=\boldsymbol{g}|_{\partial\mathcal{J}_\alpha(\boldsymbol{g},\boldsymbol{K}^{(n)})/\partial\boldsymbol{g}=0}=\left[\frac{1}{\alpha}\boldsymbol{\Psi}^T\boldsymbol{\Psi}+\left(\boldsymbol{K}^{(n)}\right)^H\boldsymbol{K}^{(n)}\right]^{-1}\left(\boldsymbol{K}^{(n)}\right)^H\boldsymbol{s} \tag{14}$$

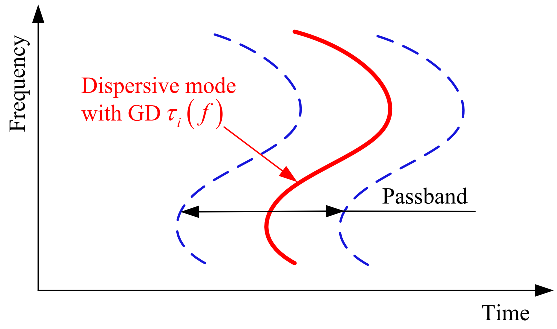

Fig. 3. Illustration of the frequency-varying filter.

where superscripts H and (n) denote the conjugate transpose and iteration counter, respectively. $\boldsymbol{K}^{(n)}$is constructed (see Eqs. (11) and (12)) with the most recent updated GDs denoted by $\tau_i^{(n)}(f)$for $i = 1, \cdots, M$. Each signal mode can then be separated as:

$$\boldsymbol{s}_i^{(n+1)} = \boldsymbol{K}_i^{(n)} \boldsymbol{g}_i^{(n+1)} \tag{15}$$

where $\boldsymbol{K}_i^{(n)}$denotes the sub-matrix of $\boldsymbol{K}^{(n)}$(see Eq. (11)). Note that Eqs. (14) and (15) essentially act as a frequency-varying filter for dispersive mode extraction as illustrated in Fig. 3. The filter bandwidth is determined by the weighting factor α. With the decreasing of α, the smoothness of the output signal will increase (indicating a decreasing filter bandwidth) [29,35].

According to Eq. (8), the GD estimation errors (i.e., $\tau_i(f) - \bar{\tau}_i(f)$in Eq. (8)) can be recovered from the phase of the dispersion-compensated signal mode $G_i(f)$. In the n-th iteration, $G_i^{(n+1)}(f)$is updated by Eq. (14), and then the GD errors can be obtained as:

$$\Delta\tau_i^{(n+1)}(f) = -\frac{1}{2\pi}\left\{\frac{\mathrm{d}}{\mathrm{d}f}\left\{\mathrm{unwrap}\left[\angle G_i^{(n+1)}(f)\right]\right\}\right\} \tag{16}$$

where $\angle$denotes the phase angle, unwrap$\{\cdot\}$denotes the phase unwrapping. Considering the noise interference, $\Delta\tau_i^{(n+1)}(f)$in Eq. (16) is preprocessed with a low-pass filter at first. Then, the GD is finally updated as:

$$\boldsymbol{\tau}_i^{(n+1)} = \boldsymbol{\tau}_i^{(n)} + \underbrace{\left[\frac{1}{\upsilon}\boldsymbol{\Lambda}^T\boldsymbol{\Lambda} + \boldsymbol{E}\right]^{-1}}_{\text{low-passfiltering}} \Delta\boldsymbol{\tau}_i^{(n+1)} \tag{17}$$

where $\Delta\boldsymbol{\tau}_i^{(n+1)} = [\Delta\tau_i^{(n+1)}(f_0), \cdots, \Delta\tau_i^{(n+1)}(f_{N-1})]^T$, $\boldsymbol{\tau}_i^{(n)} = [\tau_i^{(n)}(f_0), \cdots, \tau_i^{(n)}(f_{N-1})]^T$, $\boldsymbol{E}$is an identity matrix, $\upsilon$is a weighting factor controlling the smoothness of the output GD (υdecreases, smoothness increases) [40]. The newly estimated GD $\tau_i^{(n+1)}(f)$can be used to update the matrix $\boldsymbol{K}^{(n+1)}$(see Eqs. (11) and (12)), and then Eq. (14)~(17) can be executed again in next iteration. The iterative algorithm can be stopped when there are nearly no changes of the extracted modes between two consecutive iterations. Note that the above algorithm is designed to extract dispersive modes in the frequency domain. The time-domain waveforms of the modes can then be recovered by using the inverse Fourier transform. The flow chart of the proposed GDMD is illustrated in Fig. 4.

As shown in Fig. 4, the output results of the GDMD include the GDs $\tilde{\tau}_i(f)$and the dispersive modes $\tilde{S}_i(f)$for $i = 1, \cdots, M$. Then, the amplitude functions (see Eq. (5)) can be estimated by taking the modulus of the modes as $\tilde{A}_i(f) = |\tilde{S}_i(f)|$. With the amplitudes and GDs, a high-quality TFD of the multimodal dispersive signal can be constructed as:

$$\mathrm{TFD}(t, f) = \sum_{i=1}^{M} \tilde{A}_i(f)\delta[t - \tilde{\tau}_i(f)] \tag{18}$$

where $\delta(\cdot)$stands for the Dirac delta function defined as:

$$\delta(t) = \begin{cases} 1, t = 0 \\ 0, t \neq 0 \end{cases} \tag{19}$$

Since the GDMD adopts a joint-estimation scheme to resolve overlapped signal modes, the number of the modes, i.e., M should be specified in advance similar to the VMD and VNCMD [27,28]. In practical applications, one can determine a proper M according to the prior information of the signal or by dint of other signal processing tools like TFA [41]. In addition, one should input the weighting factors $\alpha$and υwhich regulate the smoothness of the output signal modes and the GDs, respectively (i.e., control the filter bandwidth). The GDMD can capture more details (especially for signals with complicated GDs) with the increasing of the factors. However, the output results will be less smooth in a noisy environment

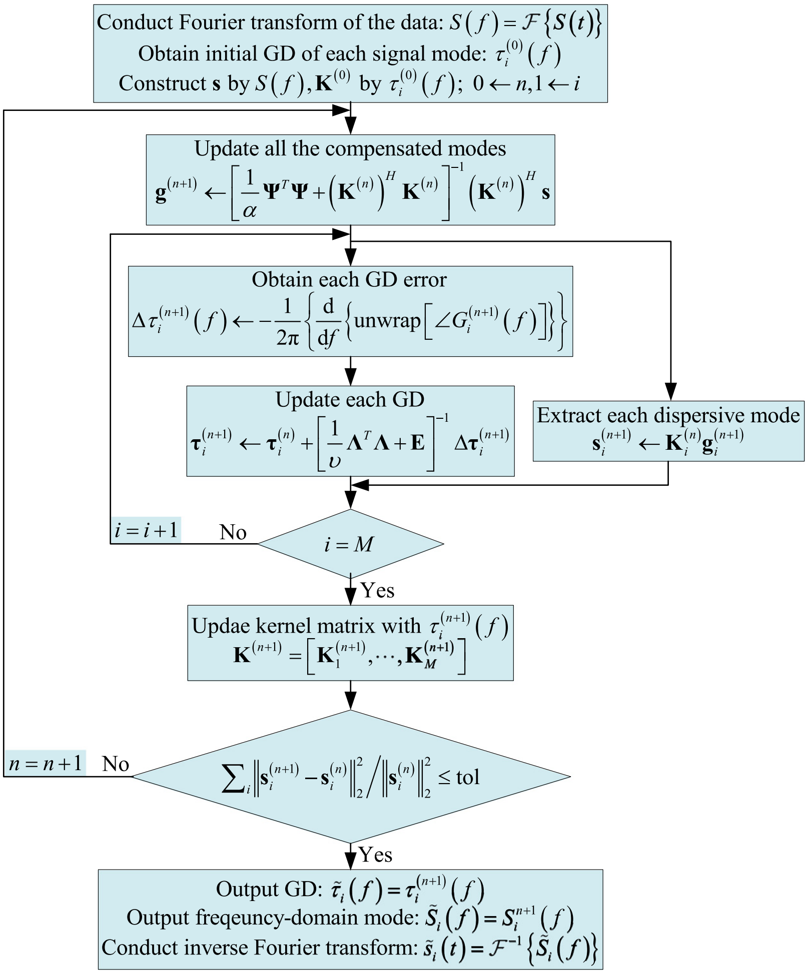

Fig. 4. Flow chart of the proposed GDMD.

with too large weighting factors. In most applications, it is suggested that $1\mathrm{e}-6\le\alpha\le1\mathrm{e}-2$, $1\mathrm{e}-8\le\upsilon\le1\mathrm{e}-5$according to different signal characteristics and noise levels. More discussions about the setting of the weighting factors can be found in [29,30]. As for the GD initialization, one may get good initial values for nearly constant GDs by detecting peaks of the time-domain signal waveform. For frequency-varying GDs, proper initial values can also be obtained by detecting ridge curves of a TFD of the signal [42].

4. Numerical examples

Numerical examples are provided to show the advantages of the proposed GDMD in this section. Hereinafter, without special note, all the simulations are carried out with MATLAB (R2010b) on a PC with a 2.6-GHz CPU. Firstly, a simulated dispersive signal containing three crossed modes is considered as:

$$S(f)=S_1(f)+S_2(f)+S_3(f),\ 0\le f\le 50\text{Hz} \tag{20}$$

$$\begin{cases}S_1(f)=1.5\exp\left[-\mathrm{j}2\pi\left(-\frac{1}{375}f^3+0.2f^2+6f+0.3\right)\right]\\ S_2(f)=\left[1+0.2\cos\left(\frac{2\pi}{25}f\right)\right]\times\exp\left[-\mathrm{j}2\pi\left(\frac{1}{375}f^3-0.2f^2+10.5f+0.5\right)\right]\\ S_3(f)=\left[1+0.2\sin\left(\frac{2\pi}{25}f\right)\right]\times\exp\left[-\mathrm{j}2\pi\left(-\frac{1}{750}f^3+12f+0.8\right)\right]\end{cases} \tag{21}$$

where the three signal modes are denoted by m1, m2, and m3, respectively, the GDs of the modes are $\tau_1(f)=-f^2/125+0.4f+6$, $\tau_2(f)=f^2/125-0.4f+10.5$, and $\tau_3(f)=-f^2/250+12$. The sampling frequency is set to 100 Hz. The signal is illustrated in Fig. 5where the time-domain waveform is obtained by applying the inverse Fourier transform to the frequency-domain signal in Eq. (20). As shown in the TFD obtained by STFT (see Fig. 5(b)), the GD curves of these modes cross with each other, and it is difficult to accurately separate these modes by existing methods.

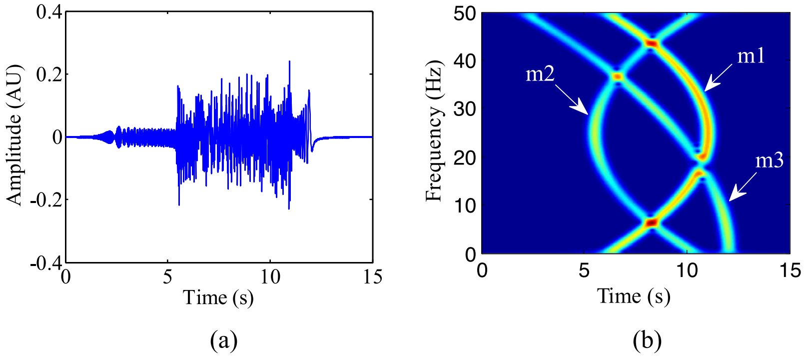

Fig. 5. The dispersive signal given in Eq. (20). (a) Time-domain waveform. (b) STFT.

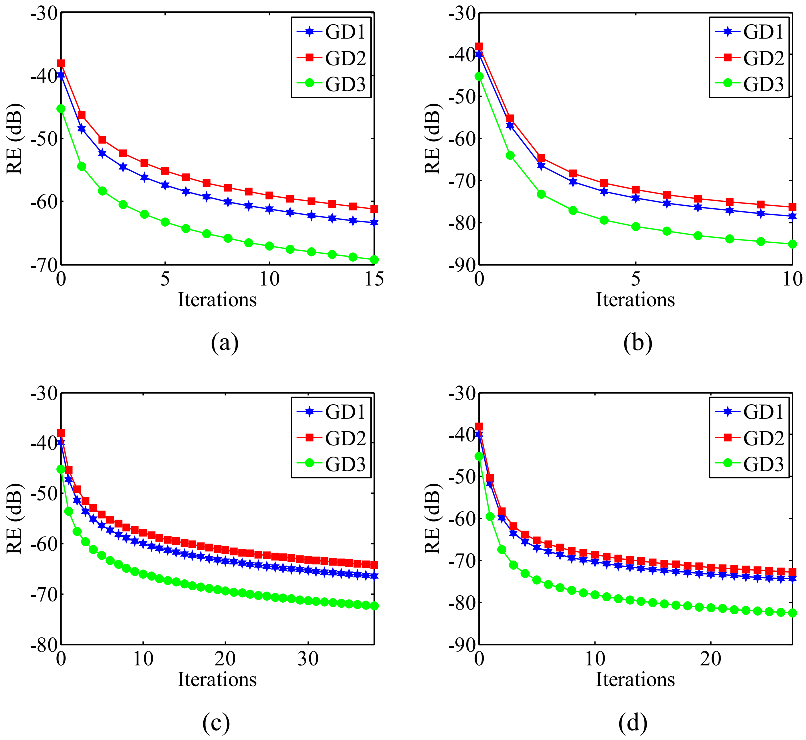

Fig. 6. REs of the estimated GDs (versus iterations) by GDMD with different parameter settings for the signal in Eq. (20) (GD1, GD2, and GD3 stand for the GDs of m1, m2, and m3, respectively). (a) $\alpha = 1e-3$, $\upsilon = 1e-7$. (b) $\alpha = 1e-3$, $\upsilon = 1e-5$. (c) $\alpha = 1e-4$, $\upsilon = 1e-7$. (d) $\alpha = 1e-4$, $\upsilon = 1e-5$.

The GDMD is employed to analyze this complicated dispersive signal. The relative error (RE) is defined to evaluate the accuracy of the GD estimation as (unit: dB):

$$\mathrm{RE} = 10\log_{10}\left\{\frac{\|\tilde{\tau}(f) - \tau(f)\|_2^2}{\|\tau(f)\|_2^2}\right\} \tag{22}$$

where $\tilde{\tau}(f)$denotes the estimated GD, $\tau(f)$stands for the true one. The initial values of the crossed GDs are obtained using the TF ridge path regrouping algorithm in [42]. Herein the convergence tolerance level is set to tol $= 1e-8$(see Fig. 4), and different weighting factors (i.e., $\alpha = 1e-3$, $1e-4$; $\upsilon = 1e-5$, $1e-7$) are adopted. Under different parameter settings, the GDMD iterates different times until the terminal condition is satisfied. Fig. 6illustrates the REs of the estimated GDs versus iterations for the GDMD. It can be observed that, for different parameter settings, the GD estimation errors all rapidly decrease to very small values with the increasing of the iterations, showing a good convergence performance of the GDMD. It also shows that, in the noise-free case, the GDMD with larger weighting factors converges faster since it has larger bandwidth for the error compensation. The results in Fig. 6 demonstrate that the GDMD can accurately estimate GDs of crossed dispersive modes.

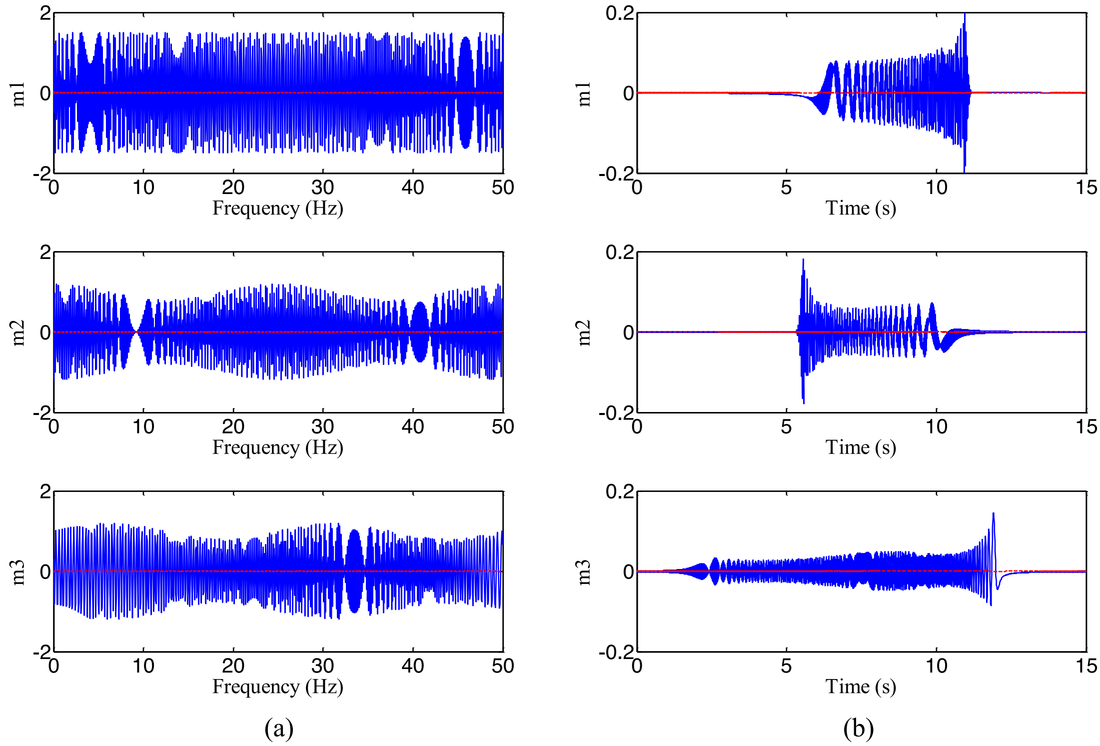

Fig. 7. Mode separation by GDMD for the signal in Eq. (20) (blue solid: estimated modes; red dashed: estimation errors). (a) Frequency-domain modes (real part). (b) Time-domain modes.

Then, the mode separation performance of the GDMD is tested as shown in Fig. 7 where both of the reconstructed frequency-domain and time-domain modes are provided. Herein the weighting factors in Fig. 6(a), i.e., $\alpha = 1e-3$, $\upsilon = 1e-7$are adopted. It can be seen that, with the joint-estimation scheme of the GDMD, these overlapped modes can be fully separated with high precision both in time and frequency domains. For comparison, the well-known DCM [32] designed for dispersive mode separation is applied to analyze the multimodal signal as shown in Fig. 8. Since the DCM adopts a short-time window to separate the dispersion-compensated modes, it will include all the signal contents near the intersections when dealing with crossed modes. As a result, the DCM introduces large mode reconstruction errors where the modes are crossing. In addition, the DCM suffers from severe end effects (in frequency domain; see Fig. 8(a)) due to the limitation of the time window.

Next, the noise robustness of the algorithm is evaluated. First, the signal-to-noise ratio (SNR) is adopted to quantify the noise level as (unit: dB):

$$\mathrm{SNR} = 10\log_{10}\left\{\frac{\|S(f)\|_2^2}{\left\|\bar{S}(f) - S(f)\right\|_2^2}\right\} \tag{23}$$

where $\bar{S}(f)$stands for the noisy signal, $S(f)$denotes the theoretical one. Then, a white Gaussian noise is added to the signal in Eq. (20) and the SNR of the obtained signal is 0 dB as shown in Fig. 9(a). The GDMD is employed to analyze such a severely polluted signal. To reduce the noise interference, relatively small weighting factors, i.e., $\alpha = 1e-5$, $\upsilon = 1e-7$are employed in this case. Due to the limited space, instead of showing each extracted signal mode, the sum of these obtained modes (SNR: 12.95 dB) by GDMD is illustrated in Fig. 9(b). It can be seen that, owing to the frequency-varying filtering property (see Fig. 3), the GDMD can effectively exclude the noise and thus significantly enhance the SNR. It indicates that the GDMD can be used as a powerful dispersive signal de-noising tool.

Then, to evaluate the performance of the TF representation, the TFD obtained by GDMD for the noisy dispersive signal is compared with that by the SST, as shown in Fig. 10. Since the noise affects the local energy distribution of the signal, the TFD by SST shows non-smooth oscillating patterns (see Fig. 10(a)). Conversely, the TFD by GDMD accurately represents the smooth GD curves of the crossed modes and also clearly reveals their energy variations (see Fig. 10(b)). In this case, the GDMD takes about 3.78 s to generate the TFD while the SST takes about 6.23 s.

To further show the advantages of the GDMD in noisy signal processing, we consider different input SNR levels and compare the SNRs of the output signals by GDMD and DCM in Fig. 11. It can be seen that the GDMD obtains much better de-noising results than the DCM especially when the input SNR is relatively high. It is because that the DCM cannot fully

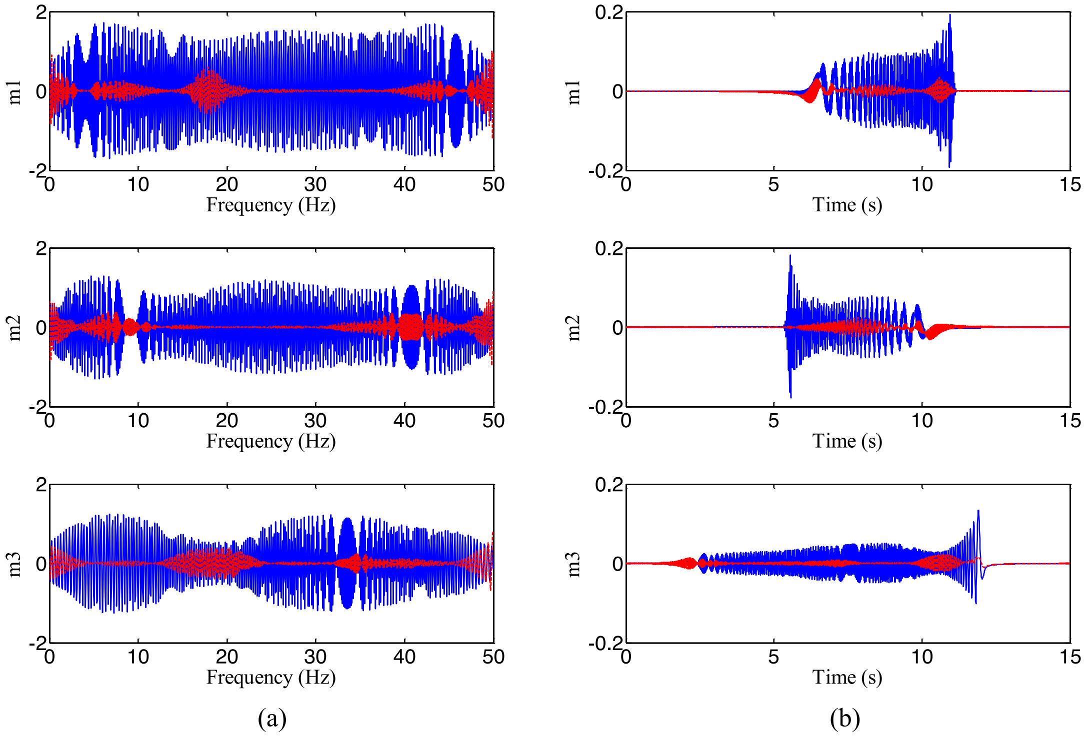

Fig. 8. Mode separation by DCM for the signal in Eq. (20) (blue solid: estimated modes; red dashed: estimation errors). (a) Frequency-domain modes (real part). (b) Time-domain modes.

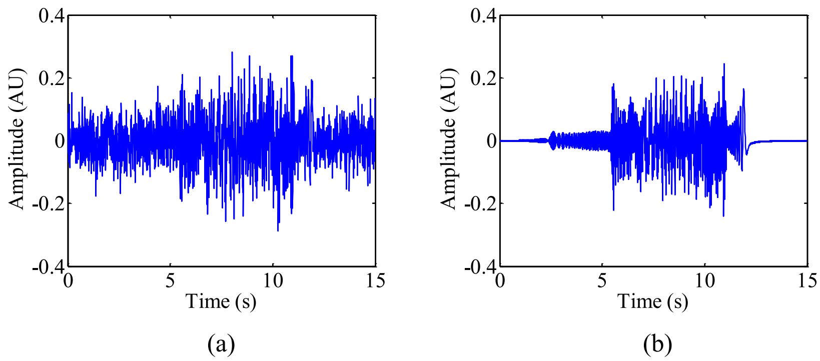

Fig. 9. Reconstruction of the signal in Eq. (20) with a 0-dB noise. (a) Original signal. (b) Reconstructed signal by GDMD (SNR: 12.95 dB).

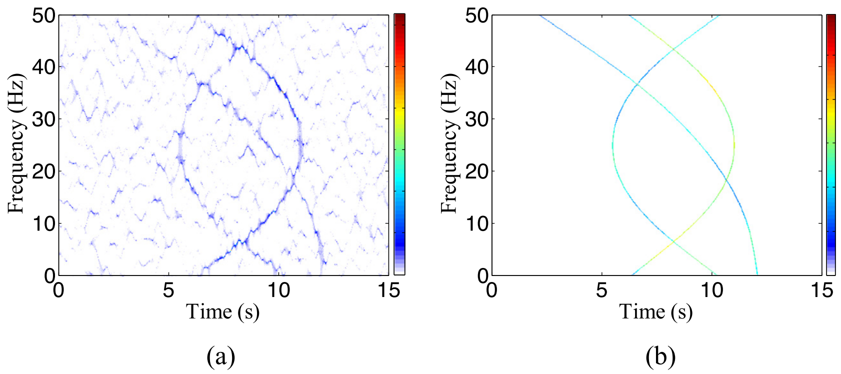

Fig. 10. Comparison of the TFDs of the signal in Eq. (20) with a 0-dB noise by (a) SST and (b) GDMD .

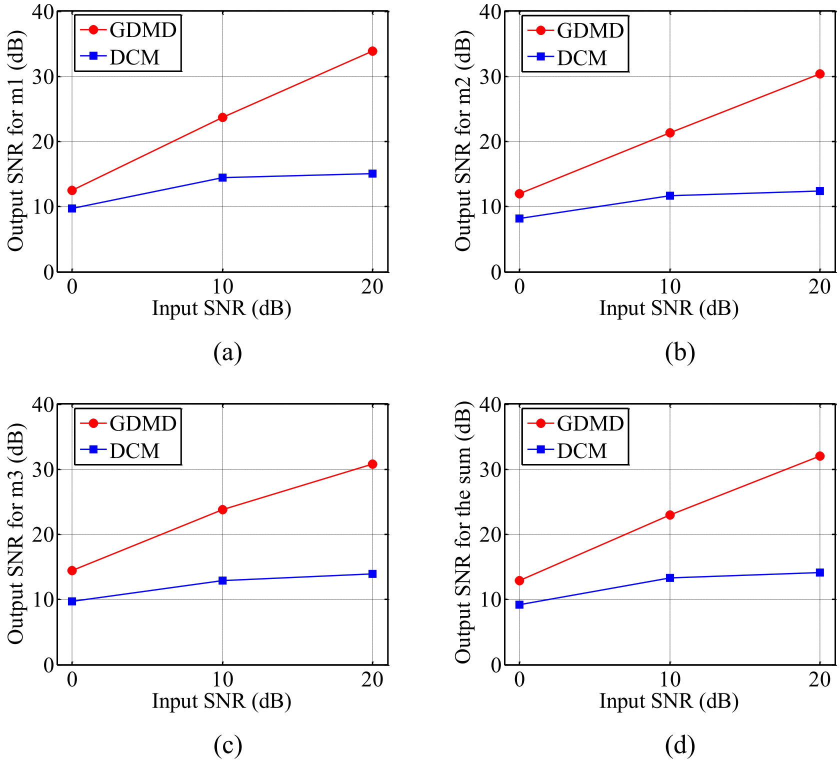

Fig. 11. Output SNRs of (a) m1, (b) m2, (c) m3, and (d) their sum by DCM and GDMD at different input SNR levels for the signal in Eq. (20).

separate overlapped modes and the resulting errors become more obvious when there is less noise. In next section, practical dispersive signals will be analyzed to demonstrate the effectiveness of the GDMD in industrial applications.

5. Real-life applications

5.1. Railway wheel fault diagnosis

Rail traffic plays a significant role in our daily life due to its strong transportation capability, good punctuality, high security and etc. For a railway vehicle, one of the most important components is the wheel whose performance directly affects the running stability and security of the vehicle. When a local defect occurs on the wheel (e.g., wheel flat), it will cause a huge impact on the rail-wheel interface, resulting in damage to the track and other components of the vehicle [43]. It is worth noting that the transient impulse response caused by the local defect can be characterized by the GDM with a relatively constant GD as defined in Eq. (5). Therefore, the proposed GDMD is applied to railway wheel fault detection in this subsection.

Herein, a track inspection vehicle with a local wheel defect is considered, as shown in Fig. 12. The wheel defect will cause abnormal vibration of the vehicle and thus seriously affect the accuracy of the track inspection. Hence, wheel fault detection is necessary. The speed (denoted by v) of the vehicle is 20 km/h and the radius (denoted by R) of the wheel is 0.16 m. The repetition time (RT) of the impulse signals caused by the wheel defect can thus be calculated as:

$$\mathrm{RT} = \frac{2\pi R}{v} = \frac{2\pi \times 0.16}{20/3.6} \approx 0.18\mathrm{s} \tag{24}$$

For the fault diagnosis, the vibration signal of the vehicle is acquired by accelerometers, as shown in Fig. 13. It can be seen that some impulse contents can be observed indistinctly, however, the repetition feature of the impulses cannot be clearly obtained due to the interference of the noise. Then, the GDMD is applied to extract the impulse signals caused by the wheel defect. For comparison, we also consider the well-known kurtosis-guided band-pass filtering method [44] which is widely used for fault diagnosis of rotary machines, as shown in Fig. 14. It can be found that the obtained fault signal by kurtosis-based filtering method is still noisy since it cannot remove the in-band noise. On the contrary, the GDMD can effectively remove the in-band noise and the RT of the impulses can be clearly indentified (see Fig. 14(b)). The detected RT matches with the theoretical one calculated in Eq. (24), indicating the presence of a local defect on the wheel. The comparison of the TFDs of the vibration signal is provided in Fig. 15. It shows that the TFD obtained by SST suffers from severe energy diffusion and thus gets very blurred. The GDMD can successfully characterize the transient impulses and thus

Fig. 12. Vibration measurement of a track inspection vehicle with a wheel defect. (a) The vehicle. (b) Wheel defect. (c) Measurement position.

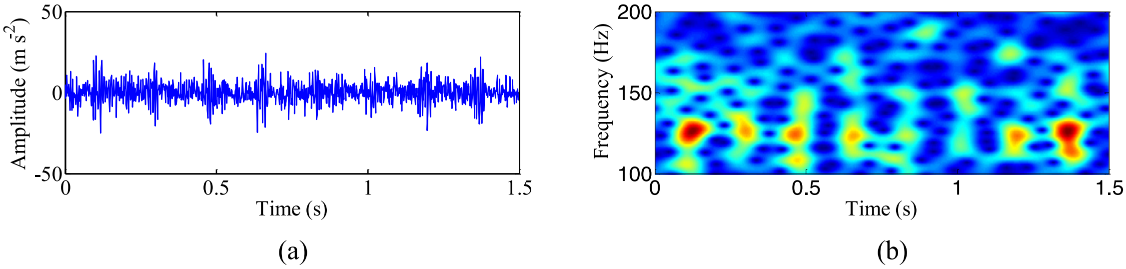

Fig. 13. Measured vibration signal of the vehicle. (a) Time-domain waveform. (b) STFT.

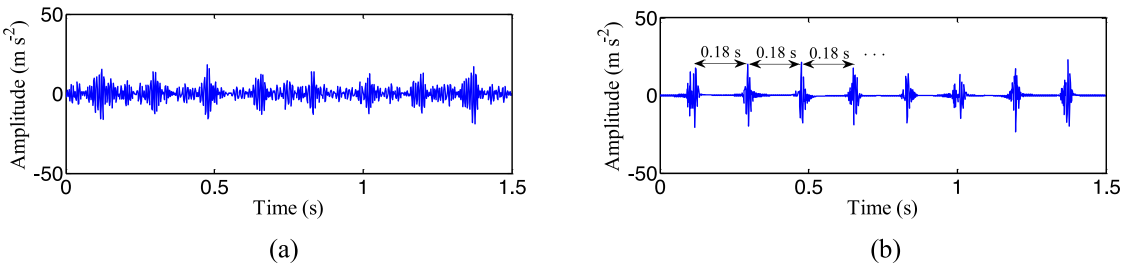

Fig. 14. Extraction of the impulse fault signal of the vehicle. (a) Kurtosis-based filtering method (center frequency 117.19 Hz; bandwidth 78.13 Hz). (b) GDMD (the sum of the 8 extracted impulse signals).

generate a high-resolution TFD for the fault signal. This example effectively demonstrates the potential application prospect of the GDMD in machine fault diagnosis. In this case, the computation time of the GDMD and SST is 5.21 s and 3.67 s, respectively. The GDMD takes a little bit more time due to the relatively large number of the signal modes (i.e., 8 signal modes).

5.2. Lamb wave signal analysis

Lamb wave is a typical guided wave which propagates in a thin plate. Due to its low attenuation rate in long distance propagation, Lamb wave has been widely applied in nondestructive testing and structure health monitoring. Lamb wave signal is usually composed of anti-symmetric and symmetric modes, denoted by $A_i$and $S_i$with the order of $i = 0, 1, \cdots$, respectively. These modes exhibit strong dispersion properties and often overlap in the TF domain. How to accurately separate these dispersive modes and extract their dispersion curves (or GD curves) has always been the difficulty in practical applications. In this subsection, the proposed GDMD is applied to address this challenging issue.

Herein, the experimental Lamb wave signal is excited and collected by a point source and receiver, laser system [10,11], as shown in Fig. 16. The experimental specimen is an aluminum alloy plate with the thickness of 3.7 mm. The Lamb wave is collected on the path with the propagation distance of 145 mm. Due to the limited frequency measurement range of the laser system, the system will cause inaccurate measurement results for some high-frequency signal components. Therefore,

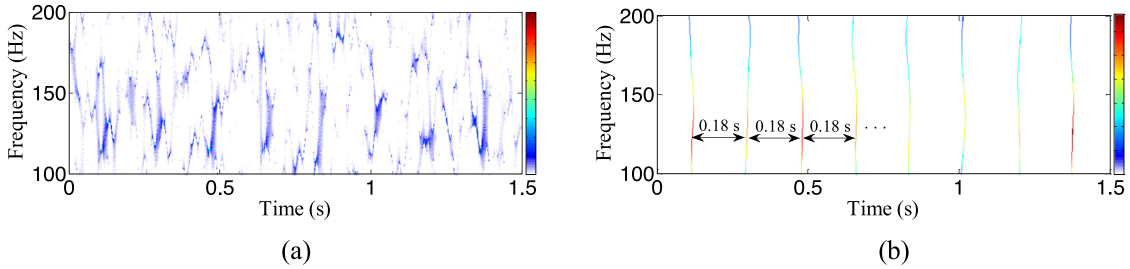

Fig. 15. Comparison of the TFDs of the vehicle vibration signal by (a) SST and (b) GDMD.

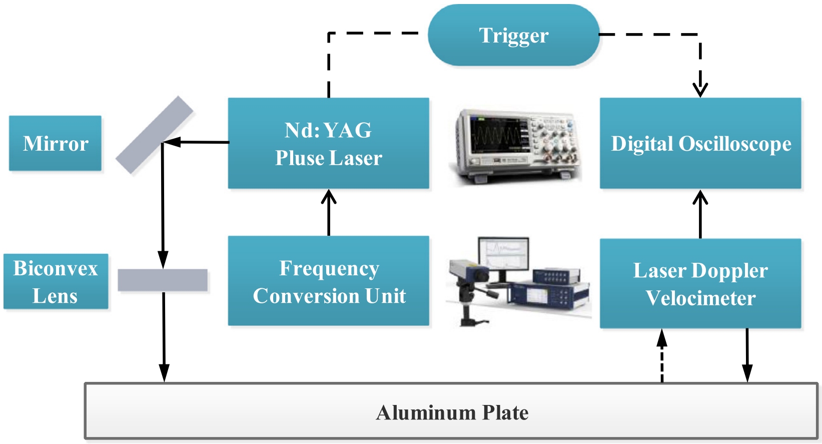

Fig. 16. Schematic diagram of the laser measurement system.

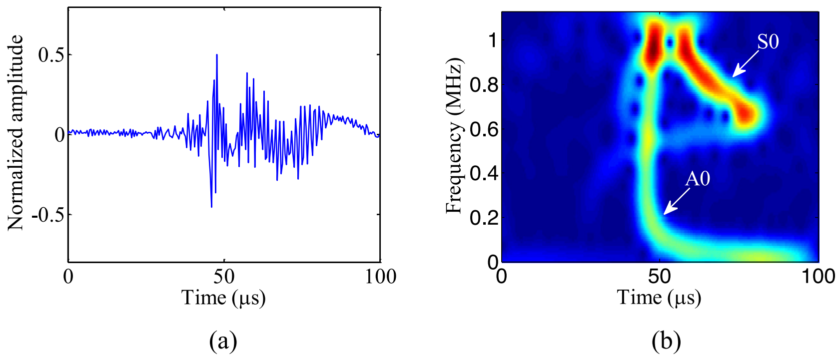

Fig. 17. Experimental Lamb wave signal (0~1.1 MHz). (a) Time-domain waveform. (b) STFT.

only the measured Lamb wave signal in the range of 0~1.1 MHz is considered, as shown in Fig. 17. It can be seen that the considered signal contains the A0 and S0 modes which are overlapped in the TF plane and the resolution of STFT is not enough to clearly represent the modes.

Then, the GDMD is applied to analyze the experimental Lamb wave signal. The overlapped signal modes are separated as shown in Fig. 18. It can be seen that, at around 50μs, the A0 mode exhibits transient impulse behaviors which well match with its TF patterns in Fig. 17(b). To further show the accuracy of the mode separation, the sum of the obtained modes is compared with the original signal, and the results obtained by DCM are also provided for comparison, as shown in Fig. 19. It can be observed that there exist large deviations between the reconstructed and the original signals during 50$-$100μsfor the DCM (see Fig. 19(a)). As for the GDMD, considering that some noise components have been filtered out, the reconstructed signal on the whole matches with the original signal well (see Fig. 19(b)). Finally, the TFDs of the Lamb wave signal obtained by SST and GDMD are compared in Fig. 20. It shows that the TFD by SST is subjected to severe energy spread especially for the A0 mode which displays transient features at $t = 50\mu$s. Conversely, the TFD by GDMD can clearly represent the two overlapped signal modes. This example demonstrates the effectiveness of the GDMD in the analysis of

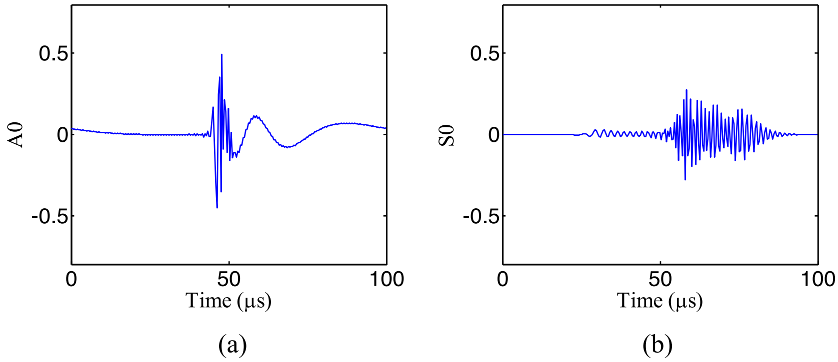

Fig. 18. Mode separation by GDMD for the Lamb wave signal. (a) A0 mode. (b) S0 mode.

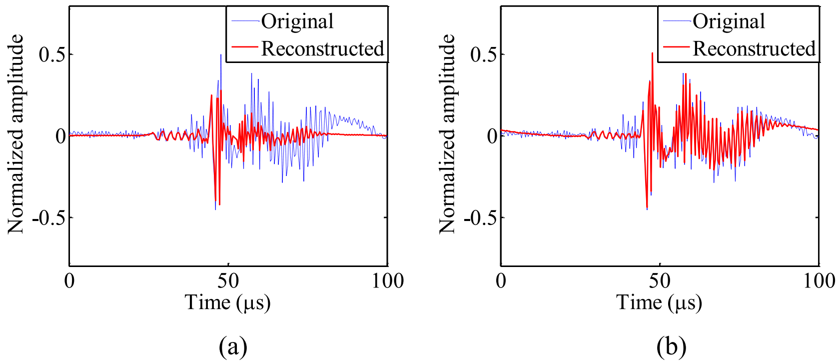

Fig. 19. Comparison of the reconstructed Lamb wave signals by (a) DCM and (b) GDMD.

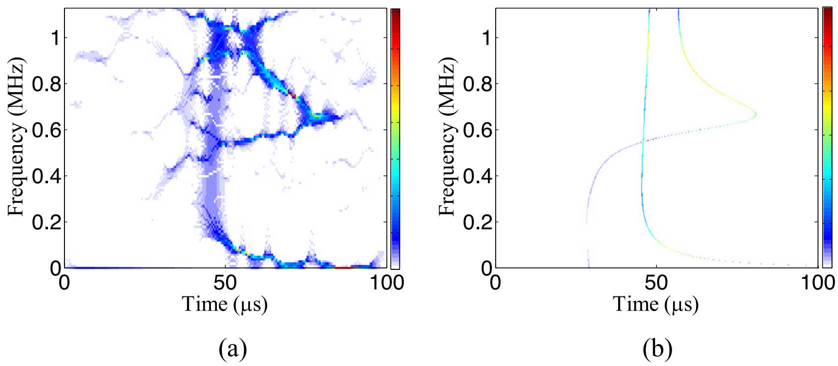

Fig. 20. Comparison of the TFDs of the Lamb wave signal by (a) SST and (b) GDMD.

practical dispersive signals with strong dispersion properties. In this case, the computation time of the GDMD and SST is 1.42 s and 1.34 s, respectively.

6. Conclusions

In this paper, a powerful signal decomposition method called GDMD has been developed to fully separate multimodal dispersive signals with crossed modes and accurately estimate their GDs. A general dispersive signal model called GDM has been defined at first. Then, the GDMD has been formulated as an optimal DCM which can be effectively solved by an iterative joint-estimation algorithm. Simulation and comparison results with the DCM and SST have been provided showing that the GDMD has higher accuracy for the separation of overlapped dispersive modes, better de-nosing performance at different SNR levels, and higher resolution for the TF representation of dispersive signals. Real-life applications in railway wheel fault diagnosis and Lamb wave signal analysis have also been carried out, demonstrating that the GDMD can not only characterize transient impulse fault signals but also guided waves with strong dispersion properties.

Declaration of Competing Interest

The authors declare that there is no competing interest in the publication of this work. All the authors have approved the submission of the manuscript to this journal.

CRediT authorship contribution statement

Shiqian Chen: Conceptualization, Methodology, Software, Writing - original draft. **Kaiyun Wang:** Resources, Funding acquisition, Writing - review & editing. **Zhike Peng:** Conceptualization, Writing - review & editing. **Chao Chang:** Validation, Investigation. **Wanming Zhai:** Supervision, Project administration.

Acknowledgments

This work is supported by the Sichuan Science and Technology Program (Grant no. 2020YJ0213), the National Natural Science Foundation of China (Grant No. 51735012), the State Key Laboratory of Traction Power (Grant no. 2020TPL-T 11), and the Key Laboratory of Urban Rail Transit Intelligent Operation and Maintenance Technology & Equipment of Zhejiang Province, Zhejiang Normal University (Grant no. ZSDRTKF2020002).

References

[1] P. Ochoa, R.M. Groves, R. Benedictus, Effects of high-amplitude low-frequency structural vibrations and machinery sound waves on ultrasonic guided wave propagation for health monitoring of composite aircraft primary structures, J. Sound Vib. 475 (2020) 115289, doi:10.1016/j.jsv.2020.115289.
[2] M. Cong, X. Wu, R. Liu, Dispersion analysis of guided waves in the finned tube using the semi-analytical finite element method, J. Sound Vib 401 (2017) 114–126, doi:10.1016/j.jsv.2017.04.037.
[3] R. Howard, F. Cegla, On the probability of detecting wall thinning defects with dispersive circumferential guided waves, Ndt E Int 86 (2017) 73–82, doi:10.1016/j.ndteint.2016.11.011.
[4] K.A. Tiwari, R. Raisutis, V. Samaitis, Hybrid signal processing technique to improve the defect estimation in ultrasonic non-destructive testing of composite structures, Sensors 17 (12) (2017) 2858, doi:10.3390/s17122858.
[5] L. Zeng, J. Lin, J. Bao, R. Joseph, L. Huang, Spatial resolution improvement for Lamb wave-based damage detection using frequency dependency compensation, J. Sound Vib 394 (2017) 130–145, doi:10.1016/j.jsv.2017.01.031.
[6] I.A. Udovydchenkov, Array design considerations for exploitation of stable weakly dispersive modal pulses in the deep ocean, J. Sound Vib 400 (2017) 402–416, doi:10.1016/j.jsv.2017.03.035.
[7] X. Tu, A. Song, X. Xu, Time reversal based frequency-domain equalization for underwater acoustic single-carrier transmissions, J. Acoust. Soc. Am. 143 (3) (2018) 1957–1958, doi:10.1121/1.5036431.
[8] Q. Vallet, N. Bochud, C. Chappard, P. Laugier, J.-.G. Minonzio, In vivo characterization of cortical bone using guided waves measured by axial transmission, IEEE Trans. Ultrason. Ferroelectr. Freq. Control 63 (9) (2016) 1361–1371, doi:10.1109/TUFFC.2016.2587079.
[9] H. Zhang, S. Wu, D. Ta, K. Xu, W. Wang, Coded excitation of ultrasonic guided waves in long bone fracture assessment, Ultrasonics 54 (5) (2014) 1203–1209, doi:10.1016/j.ultras.2013.10.020.
[10] Y. Yang, Z. Peng, W. Zhang, G. Meng, Frequency-varying group delay estimation using frequency domain polynomial chirplet transform, Mech. Syst. Signal Process. 46 (1) (2014) 146–162, doi:10.1016/j.ymssp.2014.01.002.
[11] Y. Yang, Z. Peng, W. Zhang, G. Meng, Z.Q. Lang, Dispersion analysis for broadband guided wave using generalized warblet transform, J. Sound Vib 367 (2016) 22–36, doi:10.1016/j.jsv.2015.12.037.
[12] J. He, C.A.C. Leckey, P.E. Leser, W.P. Leser, Multi-mode reverse time migration damage imaging using ultrasonic guided waves, Ultrasonics 94 (2019) 319–331, doi:10.1016/j.ultras.2018.08.005.
[13] F. Auger, P. Flandrin, Y. Lin, S. Mclaughlin, S. Meignen, T. Oberlin, H. Wu, Time-frequency reassignment and synchrosqueezing: an overview, IEEE Signal Process. Mag. 30 (6) (2013) 32–41, doi:10.1109/MSP.2013.2265316.
[14] I. Daubechies, J. Lu, H. Wu, Synchrosqueezed wavelet transforms: an empirical mode decomposition-like tool, Appl. Computat. Harmon. Anal. 30 (2) (2011) 243–261, doi:10.1016/j.acha.2010.08.002.
[15] Z. Feng, X. Chen, M. Liang, Iterative generalized synchrosqueezing transform for fault diagnosis of wind turbine planetary gearbox under nonstationary conditions, Mech. Syst. Signal Process. 52 (2015) 360–375, doi:10.1016/j.ymssp.2014.07.009.
[16] X. Chen, Z. Feng, Iterative generalized time-frequency reassignment for planetary gearbox fault diagnosis under nonstationary conditions, Mech. Syst. Signal Process. 80 (2016) 429–444, doi:10.1016/j.ymssp.2016.04.023.
[17] J. Shi, M. Liang, D. Necsulescu, Y. Guan, Generalized stepwise demodulation transform and synchrosqueezing for time–frequency analysis and bearing fault diagnosis, J. Sound Vib 368 (2016) 202–222, doi:10.1016/j.jsv.2016.01.015.
[18] D. Pham, S. Meignen, High-Order Synchrosqueezing Transform for Multicomponent Signals Analysis—With an Application to Gravitational-Wave Signal, IEEE Trans. Signal Process 65 (12) (2017) 3168–3178, doi:10.1109/TSP.2017.2686355.
[19] S. Wang, X. Chen, I.W. Selesnick, Y. Guo, C. Tong, X. Zhang, Matching synchrosqueezing transform: a useful tool for characterizing signals with fast varying instantaneous frequency and application to machine fault diagnosis, Mech. Syst. Signal Process. 100 (2018) 242–288, doi:10.1016/j.ymssp.2017.07.009.
[20] D. He, H. Cao, S. Wang, X. Chen, Time-reassigned synchrosqueezing transform: the algorithm and its applications in mechanical signal processing, Mech. Syst. Signal Process 117 (2019) 255–279, doi:10.1016/j.ymssp.2018.08.004.
[21] G. Yu, T. Lin, Z. Wang, Y. Li, Time-reassigned multisynchrosqueezing transform for bearing fault diagnosis of rotating machinery, IEEE Trans. Ind. Electron. (2020), doi:10.1109/TIE.2020.2970571.
[22] X. Tu, Z. He, Y. Hu, S. Abbas, F. Li, Horizontal synchrosqueezing transform: algorithm and applications, IEEE Sens. J. 20 (99) (2020) 4353–4360, doi:10.1109/JSEN.2020.2964109.
[23] Y. Yang, Z. Peng, X. Dong, W. Zhang, G. Meng, General parameterized time-frequency transform, IEEE Trans. Signal Process. 62 (11) (2014) 2751–2764, doi:10.1109/TSP.2014.2314061.
[24] J.C. Hong, K.H. Sun, Y.Y. Kim, Dispersion-based short-time Fourier transform applied to dispersive wave analysis, J. Acoust. Soc. Am. 117 (5) (2005) 2949–2960, doi:10.1121/1.1893265.
[25] K. Xu, P. Laugier, J. Minonzio, Dispersive Radon transform, J. Acoust. Soc. Am. 143 (5) (2018) 2729–2743, doi:10.1121/1.5036726.
[26] J. Gilles, Empirical wavelet transform, IEEE Trans. Signal Process. 61 (16) (2013) 3999–4010, doi:10.1109/TSP.2013.2265222.
[27] K. Dragomiretskiy, D. Zosso, Variational mode decomposition, IEEE Trans. Signal Process. 62 (3) (2014) 531–544, doi:10.1109/TSP.2013.2288675.
[28] S. Chen, X. Dong, Z. Peng, W. Zhang, G. Meng, Nonlinear Chirp Mode Decomposition: a Variational Method, IEEE Trans. Signal Process. 65 (22) (2017) 6024–6037, doi:10.1109/TSP.2017.2731300.

[29] S. Chen, Y. Yang, Z. Peng, X. Dong, W. Zhang, G. Meng, Adaptive chirp mode pursuit: algorithm and applications, Mech. Syst. Signal Process. 116 (2019) 566–584, doi:10.1016/j.ymssp.2018.06.052.
[30] S. Chen, Y. Yang, Z. Peng, S. Wang, W. Zhang, X. Chen, Detection of rub-impact fault for rotor-stator systems: a novel method based on adaptive chirp mode decomposition, J. Sound Vib. 440 (2019) 83–99, doi:10.1016/j.jsv.2018.10.010.
[31] S. Chen, M. Du, Z. Peng, M. Liang, Q. He, W. Zhang, High-accuracy fault feature extraction for rolling bearings under time-varying speed conditions using an iterative envelope-tracking filter, J. Sound Vib 448 (2019) 211–229, doi:10.1016/j.jsv.2019.02.026.
[32] K. Xu, D. Ta, P. Moilanen, W. Wang, Mode separation of Lamb waves based on dispersion compensation method, J. Acoust. Soc. Am. 131 (4) (2012) 2714–2722, doi:10.1121/1.3685482.
[33] C. Xu, Z. Yang, X. Chen, S. Tian, Y. Xie, A guided wave dispersion compensation method based on compressed sensing, Mech. Syst. Signal Process 103 (2018) 89–104, doi:10.1016/j.ymssp.2017.09.043.
[34] Z. Liu, K. Xu, D. Li, D. Ta, W. Wang, Automatic mode extraction of ultrasonic guided waves using synchrosqueezed wavelet transform, Ultrasonics 99 (2019) 105948, doi:10.1016/j.ultras.2019.105948.
[35] M.-.C. Pan, Y.F. Lin, Further exploration of Vold–Kalman-filtering order tracking with shaft-speed information—I: theoretical part, numerical implementation and parameter investigations, Mech. Syst. Signal Process. 20 (5) (2006) 1134–1154, doi:10.1016/j.ymssp.2005.01.005.
[36] S. Mallat, Z. Zhang, Matching pursuits with time-frequency dictionaries, IEEE Trans. Signal Process. 41 (12) (1993) 3397–3415, doi:10.1109/78.258082.
[37] W. Huang, G. Gao, N. Li, X. Jiang, Z. Zhu, Time-frequency squeezing and generalized demodulation combined for variable speed bearing fault diagnosis, IEEE Trans. Instrum. Meas. 68 (8) (2019) 2819–2829, doi:10.1109/TIM.2018.2868519.
[38] S. Lu, P. Zhou, X. Wang, Y. Liu, F. Liu, J. Zhao, Condition monitoring and fault diagnosis of motor bearings using undersampled vibration signals from a wireless sensor network, J. Sound Vib. 414 (2018) 81–96, doi:10.1016/j.jsv.2017.11.007.
[39] Y. Huang, J. Lin, Z. Liu, W. Wu, A modified scale-space guiding variational mode decomposition for high-speed railway bearing fault diagnosis, J. Sound Vib 444 (2019) 216–234, doi:10.1016/j.jsv.2018.12.033.
[40] M.P. Tarvainen, P.O. Rantaaho, P.A. Karjalainen, An advanced detrending method with application to HRV analysis, IEEE Trans. Biomed. Eng. 49 (2) (2002) 172–175, doi:10.1109/10.979357.
[41] S. Meignen, T. Oberlin, S. Mclaughlin, A new algorithm for multicomponent signals analysis based on synchrosqueezing: with an application to signal sampling and denoising, IEEE Trans. Signal Process. 60 (11) (2012) 5787–5798, doi:10.1109/TSP.2012.2212891.
[42] S. Chen, X. Dong, G. Xing, Z. Peng, W. Zhang, G. Meng, Separation of overlapped non-stationary signals by ridge path regrouping and intrinsic chirp component decomposition, IEEE Sens. J. 17 (18) (2017) 5994–6005, doi:10.1109/JSEN.2017.2737467.
[43] W. Zhai, Vehicle–track Coupled dynamics: Theory and Applications, Springer, Singapore, 2020, doi:10.1007/978-981-32-9283-3.
[44] J. Antoni, Fast computation of the kurtogram for the detection of transient faults, Mech. Syst. Signal Process. 21 (1) (2007) 108–124, doi:10.1016/j.ymssp.2005.12.002.